Published in final edited form as:
Radiol Clin North Am. 2008 January ; 46(1): 149–vii. doi:10.1016/j.rcl.2008.01.004.

Magnetic Resonance Imaging-guided Interventions in the Genitourinary Tract: An Evolving Concept

Fiona M. Fennessy, M.D. Ph.D., **Kemal Tuncali, M.D.**, **Paul R. Morrison, B Sc.**, and **Clare M. Tempany, M.D.**
Dept. of Radiology, Harvard Medical School/Brigham & Women's Hospital, Boston, MA

Keywords

MRI; genitourinary; MRgFUS; cryoablation; brachytherapy; fibroids; prostate; RFA

Introduction

Magnetic resonance imaging (MRI)-guided interventions are now a well-established form of routine patient care in many centers around the world. There are many different approaches, dependent upon magnet design and clinical need. The rational behind this is based initially upon the fact that MRI provides such excellent inherent tissue contrast, without ionizing radiation risk to the patient. MRI-guided minimally invasive therapeutic procedures have shown major advantages over conventional surgical procedures. In the genitourinary tract, MRI guidance can play a role in tumor detection, localization and staging and can provide accurate image guidance for minimally invasive procedures for the confirmation of pathology, tumor treatment, and treatment monitoring. Depending on the body part being accessed, a customizable magnet bore configuration and MR-compatible devices can be made available. The advent of molecular and metabolic imaging and the use of higher strength magnets will likely improve diagnostic accuracy and allow patient-specific targeted therapy, designed to maximize disease control and minimize side effects.

Genital Tract: Female

One of the most unique and exciting MR guided interventional procedures in the female pelvis is Magnetic Resonance guided Focused Ultrasound Surgery (MGgFUS). In addition, MR has been used to guide other interventions and therapies such as biopsies and MR-guided gynecological tumor treatments. The latter have been done in several centers to guide the placement of radiation catheters for delivery of high dose radiation in cervical or endometrial cancer (1).

Please send correspondence to: Fiona Fennessy, M.D. Ph.D., Department of Radiology, Brigham and Women's Hospital, 75 Francis Street, Boston, MA 02115, Tel: (617) 632 4785 Fax: (617) 632-3505 email: ffennessy@partners.org. Kemal Tuncali: Dept Radiology, Brigham and Women's Hospital, 75 Francis st, Boston, MA 02115, Ph: 617 732 6675, fax: 617 632 3505; ktuncali@partners.org. Paul Morrison: Dept Radiology, Brigham and Women's Hospital, 75 Francis st, Boston, MA 02115, Ph: 617 732 5500, ext 30210, fax: 617 632 3505; pmorrison@partners.org. Clare Tempany: Dept Radiology, Brigham and Women's Hospital, 75 Francis st, Boston, MA 02115, Ph: 617 732 8772, fax: 617 632 3505; ctempany@bwh.harvard.edu.

Magnetic Resonance guided Focused Ultrasound Surgery for treating Uterine Fibroids

Uterine fibroids are the most common female pelvic tumor, occurring in approximately 25% of women (2). While many patients remain asymptomatic, others suffer from symptoms such as pelvic pain, menorrhagia, dysmenorrhagia, dyspareunia, urinary frequency and infertility. Ultrasound is usually the first diagnostic imaging modality of choice for fibroids, demonstrating a well-defined usually hypoechoic mass. Providing good inherent tissue contrast, MRI is the optimal modality for fibroid detection, most accurate localization and volumetrics.

A wide spectrum of treatment options for uterine fibroids exists, ranging from expectant waiting to medical management to myomectomy to hysterectomy. However, women are increasingly seeking less invasive treatment options, perhaps motivated by fertility preservation and the possibility of reduced post-procedure recovery time. A good example of a less invasive choice is uterine artery embolization (UAE), a procedure that has demonstrated significant growth and interest since its first introduction in 1995 (3). However, only MRgFUS is completely non-invasive. Approved by the United States Food and Drug Administration (FDA) in October 2004, much of the worldwide experience with MRgFUS has been with treatment of uterine fibroids, with more than 3,500 patients treated to date.

Fundamentals of MRgFUS

The potential surgical application of focused ultrasound surgery (FUS) was first demonstrated in 1942 (4). Since then it has been extensively evaluated in the brain of both animals (5,6) and humans (7), and in the kidney, prostate, liver, bladder (8–11) and eye (12) within clinical trials. However, clinical acceptance was hampered due to the difficulty in controlling the focal spot position, precisely defining the beam target, and coping with the lack of feedback about thermal damage.

MR imaging can satisfy the requirements of FUS, having excellent anatomical resolution and high sensitivity for tumor visualization, thereby offering accurate planning of the tissue to be targeted. By exploiting the temperature dependence of the water proton resonant frequency (13), MR-based temperature mapping is possible. This allows for targeting of the beam during sub-threshold ultrasound exposures (14) and online estimation of the ablated volume (15,16). Phase imaging is used to estimate the temperature-dependent proton resonant-frequency shift using a fast spoiled gradient-recalled-echo sequence (SPGR) (17). Therefore, obtaining temperature-sensitive MR images before, during and after each sonication can monitor tissue temperature elevations, including any slight elevations in normal adjacent surrounding tissue, thereby preventing damage.

MRgFUS equipment for fibroid treatment

Sonications are performed using an MR-compatible focused ultrasound system that is built into a table that docks with a compatible MR scanner. The system consists of a focused piezoelectric phased-array transducer (208 elements, frequency: 0.96–1.14 MHz) that is located within the specially designed table surrounded by a water tank. A thin plastic membrane covers the water tank and allows the ultrasound beam to propagate into the tissue. The patient lies in a prone position in the magnet, with the anterior abdominal wall positioned over the water tank. The location of the focal spot is electronically controlled by the transducer array that controls the volume of coagulation necrosis.

Patient selection for MRgFUS of uterine fibroids

The FDA has currently approved this procedure for premenopausal females with symptomatic uterine fibroids who have no desire for future pregnancy. This treatment is not indicated for pregnant women, post-menopausal women, or those with contraindications to contrast-enhanced MRI. If multiple fibroids are present, clinical symptomatology and accessibility to the target fibroids is reviewed and a target fibroid is selected. The anterior abdominal wall is evaluated for extensive scarring. Those women with such scarring are excluded from treatment due to the risk of skin burns (18).

Treatment planning

Immediately prior to treatment, T2-weighted fast spin-echo images in three orthogonal planes are obtained to plan the beam path to the targeted lesion. The MR images are analyzed to evaluate the area to be treated for possible obstructions. While patients with extensive anterior abdominal wall scarring in the beam path are generally excluded at screening, it may however be possible to treat women with abdominal wall scarring that is not extensive by angling the beam path, ensuring that the scar is not traversed (Figure 1). Filling of the urinary bladder by Foley catheter clamping may also help in moving the uterus and selected fibroid into a position away from the abdominal wall scar. Coursing bowel loops lying anterior to the uterus at the level of the uterine fibroid may also cause treatment-planning difficulties. Placement of a gel spacing device may allow the bowel loops to be displaced out of the treatment field, thereby enlarging the acoustic window and allowing for greater treatment volume (Figure 2).

Clinical Trials in the treatment of uterine fibroids with MRgFUS

Multicenter clinical trials investigating the use of MRgFUS in the treatment of uterine fibroids, which subsequently resulted in device labeling by the FDA, were carried out at 5 medical centers across the US, in addition to centers in the UK, Germany and Israel. Follow-up of many of these patients is ongoing.

Enrollment for Phase I/II began in 1999 to assess the safety and feasibility of MRgFUS in the treatment of fibroids. Eligible patients underwent MRgFUS followed by hysterectomy and subsequent pathological examination of the uterus and fibroid showed that MRgFUS did indeed result in hemorrhagic necrosis in the area of non-perfusion on the post-treatment MR (19,20).

Phase III of the clinical trial involved treatment of larger volumes of fibroids in women with symptomatic uterine fibroids who would otherwise have opted for hysterectomy (Figure 3). To date, the longest-term follow-up—in 359 patients—is up to 24 months (21). These patients reported durable symptom relief. Those that had a greater non-perfused treatment volume fared better, with fewer of these patients undergoing additional fibroid treatment. These findings concur with those of Fennessy et al., where greater clinical outcome was found in those who were treated with a modified treatment protocol that allowed for greater non-perfused fibroid volumes post-treatment (22).

Cryotherapy for Uterine Fibroids

MR-guided cryotherapy is a minimally invasive procedure. It involves a percutaneous approach in an interventional setting with multiple (1–5) needle-like 17G cryotherapy probes. Each probe creates a teardrop shaped volume of frozen tissue about its tip (approximately 2.5 mm diameter); the simultaneous use of multiple probes gives a larger volume of treated tissue in the same timeframe as treating with a single probe. The freeze is provided by pressurized argon gas that circulates within the probe. Typical treatments

involve a cycling of the gas that delivers a freeze-thaw-freeze to destroy tissue; with each stage of the cycle being 10–15 minutes in duration. MRI-guided cryotherapy has been evolving through experiment and clinical use in the last 20 years to target a range of tumors in various organ systems (23). Compared to ultrasound that has shadow artifacts, visibility of the iceball for monitoring is not similarly limited.

There are many procedural reports of MRI-guided cryotherapy to treat symptomatic patients with uterine fibroids (24–27). During cryotherapy, the ice appeared as a signal void in the image due to the short MR relaxation time of the solid ice, giving a clear demarcation between frozen and unfrozen tissue. The clinical endpoint for the procedure is to fully cover the fibroid by the ice based on intra-procedural imaging. However, short term clinical outcome has only been reported in 8 of 9 treated patients, who demonstrated on average, 65% volume reduction in uterine size (25).

One of these studies (26) was performed transvaginally, with the authors proposing that such an approach had the advantage of providing direct access, especially for submucosal tumors. Procedures are usually performed with epidural anesthesia in a horizontally open MRI scanner with multiple 2–3 mm cryotherapy probes (Figure 4). Both gradient echo and T2-weighted spin-echo sequences were used to guide probe placement and monitor the treatment cycle of freeze-thaw-freeze (Figure 5).

Percutaneous ablation of fibroids is a nascent procedure and not widely practiced. This method of ablation has found a place in treating other parts of the body but not necessarily treating uterine fibroids, possibly due to the recent emergence of other minimally invasive procedures such as uterine artery embolization, or non-invasive procedures such as focused ultrasound surgery.

Genital tract: Male

The leading cause of cancer death in men over 50, prostate cancer affects one man in six in his lifetime. According to the American Cancer Society, it is estimated that in 2007 in the United States, 218,890 new cases of prostate cancer will be diagnosed, and approximately 27,050 men will die of the disease (28). There is only a 33% five-year survival in men with metastatic disease (29), making early tumor detection and localized treatment a necessity.

MRI-guided Prostate Biopsy

Early diagnosis and cancer localization within the prostate gland is usually found through digital examination, serum prostate-specific antigen (PSA) measurement, followed by transrectal ultrasound (US)-guided biopsy. Image-guided prostate biopsy with US has become a universally accepted tool (30), but because of a relatively low sensitivity and specificity of tumor detection (31), interest continues in the development of a more accurate technique. In addition, for men with increasing PSA levels and repeatedly negative transrectal US-guided prostate biopsies (the concern being that a sampling error may have resulted in a false-negative biopsy), for those in whom a transrectal biopsy is not possible, or for those who are reluctant to undergo transrectal biopsy because of its recognized complications, such as infection, hematuria, hematospermia and rectal bleeding (32–34), an alternative approach may be necessary.

MRI can clearly outline prostate architecture and substructure. While the specificity for diagnosis may be limited, MRI can demonstrate suspicious nodules in the peripheral zone, the most common site for prostate cancer. On T2weighted images, tumor is most commonly demonstrated by either focal or diffuse regions of decreased signal intensity relative to the high-signal-intensity normal peripheral zone. MRI is most routinely used for staging men

with known cancer. The reported accuracy of prostate cancer detection and staging on MR images varies widely, with reports of accuracy ranging from 54% to 93%, likely due to differences in techniques and inter-observer variability (35–38).

Its role in detection and characterization, particularly in the initial diagnosis of high-risk patients or those with previous negative biopsy findings but persistentlyhigh PSA levels is increasing, as techniques such as Spectroscopy (MRSI) and Dynamic Contrast Enhancement (DCE) become more widely available. The ultimate role and application in clinical practice, however, remains somewhat controversial (35). It has been demonstrated that MRI contributes significant incremental value to both transrectal ultrasound (TRUS) -guided biopsy and digital rectal exam in cancer detection and localization in the prostate (39). It offers an excellent second-line alternative to those who have failed to obtain a diagnosis with conventional methods.

Two basic strategies have been explored for MRI-guided prostate biopsy. The first is co-registration of previously acquired diagnostic MR images to transrectal US images, localizing suspected tumor lesions on MR and correlating these locations to the US (40). The second strategy is stereotactic needle interventions within diagnostic MR scanners using careful patient positioning. By implementing surgical navigation software originally developed for neurosurgery (41,42) and adapting the technical capabilities of MRI- guided prostate brachytherapy in an open configuration magnet (43), biopsy of suspected tumor foci in the peripheral zone is made possible (44) (Figure 6). In addition, the feasibility of transrectal needle access to prostate tumors has been assessed in a closed- bore 1.5T magnet (45–48) in a small number of patients, which could potentially provide for additional functional and spectroscopic imaging, in comparison to with a 0.5T scanner. The procedure requires the use of a specialized device that consists of a needle guide and support system. The same guidance has recently also been used in a 3T system (49). However, larger studies of clinical usefulness are necessary. With progress in biologic imaging of the prostate gland, it is likely that MRI-guidance will play an increasing role in the diagnosis and treatment of prostate cancer.

MRI-guided prostate biopsy: the future

The move towards targeted interventions, both for diagnosis and treatment, underscores the need for precise image-guided needle placement. Based on a patient's anatomy and lesion detection in a pretreatment MRI, a graphical planning interface that allows desired needle trajectories to be specified, through MR-compatible robotic assistance, has been recently described (50). Avoiding the limitations of a fixed-needle template is a positive move forward both for tissue sampling and treatment. As the field of prostate imaging moves to higher strength magnets- namely 3T, the biopsy devices are being re-configured to allow sampling in a closed-bore environment. A recent study on prostate biopsy using 3T MRI-guidance, described it as a promising tool for detecting and sampling cancerous regions in patients with known prostate cancer (49); however, the role (even at 3T) of MRI-guided prostate biopsy as a screening tool in patients with elevated PSA levels and recent previous negative biopsy remains to be determined.

MRI-guided Brachytherapy for Prostate Cancer

Established options for the management of localized prostate cancer include one or a combination of the following: radical prostatectomy, external beam radiation therapy, brachytherapy or “watchful waiting”. In radiation therapy, the goal is to achieve the prescribed dose throughout the prostate gland, while minimizing toxicity to adjacent structures and morbidity from the procedure. Prostate brachytherapy is one of the more popular radiation methods in the prostate and involves the percutaneous placement of I-125

radiation seeds into the gland under image guidance. This is most commonly done with TRUS. It can also be done with MR guidance and the goal in both procedures is to optimize seed placement and allow maximal dose to the prostate, peripheral zone and tumor and minimal dose to the urethra and rectum.

Targeted radiation therapy, therefore, allows with the guidance of imaging, directed tumor treatment, decreasing the chances of disease spreading outside the gland, while healthy prostate tissue and its neighboring structures are not overdosed. This is extremely important for structures such as the urethra in which over-radiation may cause stricture and fistualization that can be avoided with good image guidance (51,52). Radiation dose fall-off is sharp at the rectal wall and at the urethra. Unlike external beam radiotherapy, there is no entrance or exit dose. Brachytherapy, therefore, has the potential to achieve superior tumor control with decreased morbidity and side effects. It is not, however, without its own set of complications, such as rectal irritation and ulceration, incontinence and impotence due to inadvertent delivery of radiation dosing to the rectum, bladder and urethra.

Patient selection

Low-risk prostate cancer patients with a high probability of organ-confined disease are appropriately screened with an endorectal coil MR for potential treatment with brachytherapy monotherapy. Most centers include patients with stage T1-T2a (according to the American Joint Committee on Cancer/International Union Against Cancer 1997 staging), PSA level of 10 ng/mL or less, and a Gleason score of 6 or lower. The relatively few contraindications to the procedure include prior transurethral resection of the prostate (TURP) or morbid obesity (equipment cannot sustain the weight).

Procedure

MR-guided prostate brachytherapy using both open configuration 0.5T and 1.5T scanners have been described (43,45). Using the open 0.5T magnet, the patient is placed supine between the two magnets in the lithotomy position under general anesthesia. A Foley catheter is inserted, the skin is prepared and draped in a sterile fashion and a template for needle guidance is placed against the perineum. A rectal obturator is then placed and T2-WIs are acquired in the axial, coronal and sagittal planes, and used to outline the urethra, peripheral zone and anterior rectal wall. Surgical simulation software outlines these areas, and the targeted volume is calculated using designated planning software (53). Seed number and depth of catheter insertion are calculated.

While gradient-echo MR images are obtained in real-time (44), seed-loaded catheters are then positioned in the prostate gland (Figure 7). The images are then compared to their intended locations, according to the radiation therapist plan. Dose-volume histograms of the urethra, anterior rectal wall and target volume are obtained prior to final deployment of seeds. Six weeks after the procedure both CT imaging (to accurately identify the seeds) and MRI (for prostate anatomical correlation) are fused to calculate the final dose distribution to the gland and surrounding tissues.

While open-bore magnets offer good patient accessibility and allow satisfactory prostate tumor and anatomical depiction, higher quality MR intervention images in a closed 1.5T system have also been investigated (45). This system uses a customized perineal template, an endorectal imaging coil and a lockable positioning arm. The patient is placed in the left lateral decubitus position. While patient accessibility with this technique may be limited due to the closed-bore configuration and the 60cm diameter bore, the authors found that dependence on deformable registration between image sets (high-field 1.5T diagnostic images and low-field strength interventional images) was reduced.

Outcomes

Short-term toxicity after MR-guided brachytherapy is rare, with no gastrointestinal or sexual dysfunction reported during the first month after treatment (54). Within 24 hours of removal of the Foley catheter, acute urinary retention was reported in 12% of men, which was self-limited to within 1 to 3 weeks of treatment. Prostatic volume and transitional zone volume, determined by MRI, and number of brachytherapy seeds placed, were found to be significant predictors of acute urinary retention.

The long-term genitourinary and rectal toxicity was compared between those who received MR-guided brachytherapy alone, and those who received combined MR-guided brachytherapy and external beam radiation therapy (55). The 4-year estimates of rectal bleeding requiring coagulation for patients, who underwent MR-guided brachytherapy, compared with patients who received combined-modality therapy, were 8% versus 30%. The 4-year estimate of freedom from radiation cystitis was 100% versus 95% for patients who received MR-guided brachytherapy alone and patients who received combined-modality therapy, respectively. In a separate study evaluating the long-term toxicity in patients who received MR-guided brachytherapy as a salvage procedure for radiation therapy failure (56), the 4-year estimate of grade 3 or 4 gastrointestinal or genitourinary toxicity was reported at 30% of all patients, with 13% requiring an intervention such as a colostomy or urostomy for fistula repair.

Supplemental external beam radiotherapy, in addition to brachytherapy seed implantation, has been given to patients with intermediate to high-risk prostate cancer (according to the D'Amico risk stratification for prostate cancer) (57). This combination of radiation therapy has demonstrated very good long-term results (58,59), resulting in a 15-year biochemical relapse-free survival equal to 80.3% for intermediate-risk disease, and 67.2% for high-risk disease.

Brachytherapy: the future

The current manual method of needle placement, utilizing a fixed-needle template guide, constrains needle orientation. The manual method also makes use of manual computation and transcription of needle coordinates that are prone to human error. The future points towards a system that incorporates an interactive planning interface with MR-compatible robotic assistance. Such a device, which serves as a dynamic guide for precise needle placement, has been developed (60). Likely the future direction for percutaneous MRI-guided prostatic interventions, this MR-compatible robotic device has been integrated with a software planning interface, allowing the physician to specify desired needle trajectories, based on MRI anatomy.

Focused Ultrasound Surgery in the Prostate

As discussed in the preceding female genital tract section, there is growing interest in MRgFUS, due to its many potential applications as a minimally invasive therapy. Ultrasound-guided focused ultrasound surgery (USgFUS), has been used predominantly in Europe for the treatment of prostate cancer. Limitations include difficulty in treating the anterior prostate or small volume prostates and lack of long-term follow-up.

Literature describing the results of USgFUS for prostate cancer suggests that USgFUS treatment is a valuable option for well-differentiated and moderately differentiated tumors, as well as for local recurrence after external-beam radiation therapy (61–63). USgFUS treatment is whole gland therapy, without selective tumor-directed targeted treatment that should allow for minimal disruption of normal function. USgFUS is arguably limited by the lack of direct temperature and thermal dose measurements during thermocoagulation.

Without the latter, the energy delivery cannot be controlled or monitored nor can the thermal dose be accurately measured.

To address these challenges, MRI-compatible prostate applications have been developed for hyperthermia (64) and phased-array applicators for thermal ablation (65). Insightec Inc. has developed a MRI-guided focused ultrasound system for prostate treatment (Figure 8). A major potential advantage of MRI-guidance is its ability to map functional changes in prostate tissue, with the possibility of 3D tumor mapping before and during treatment. Overall, non-invasive thermal ablation using MRI-guidance, should significantly improve prostate treatment and its application should increase in the near future.

MRI-guided catheter-based Ultrasound Thermal Therapy of the Prostate

In a similar mode, catheter-based ultrasound devices (in interstitial and transurethral configurations) have been evaluated in canine prostate models *in vivo* and found to produce spatially selective regions of thermal destruction in the prostate (66–68). Transurethral ultrasound devices with tubular transducers have been developed that can coagulate sectors of the prostate using pre-shaped angular patterns (69,70). Devices with finer spatial control using planar (71,72) or curvilinear transducers (73) can be slowly rotated using a computer-controlled, MR- compatible stepper motor while under MRI guidance and feedback (Figure 9). The feasibility of MRI-guided interstitial ultrasound thermal therapy of the prostate has been evaluated in an in vivo canine prostate model (66). MRI-compatible, multi-element interstitial ultrasound applicators were utilized. The applicators were inserted transperineally into the prostate with the energy directed ventrally away from the rectum. This study demonstrated a large volume of ablated tissue within the prostate and, importantly, demonstrated contiguous zones of thermal coagulation. At least in an animal model and using MR guidance, both transurethral and interstitial treatment strategies have, therefore, demonstrated significant potential for thermal ablation of localized prostate cancer.

Urinary Tract

Renal cell carcinoma (RCC) is the sixth leading cause of cancer death, (74) and its incidence in the US is rising (75). Partial nephrectomy, a nephron-sparing surgical method has replaced radical nephrectomy for the treatment of small RCC. Less invasive methods have also emerged that can be performed laparoscopically (partial nephrectomy, cryosurgery) or percutaneously (radiofrequency ablation, cryoablation). Image-guided percutaneous ablations have the potential to replace others as the least invasive and least costly (76) of all nephron-sparing treatments clinically available, particularly in patients who are poor surgical candidates due to co-morbid disease as well as in patients with renal insufficiency, solitary kidney, or multiple RCC.

MRI-guided Radiofrequency Ablation in the Kidney

Radiofrequency ablation (RFA) is a focal thermal tumor therapy method in which tissue is heated by an electrical current. The current is present with a high density surrounding a percutaneously placed electrode that is driven by an electrical generator. The circuit is completed by the placement of “grounding pads” on the patient. The electrode is placed interstitially and intended to be activated to create a volume of coagulative necrosis in place of the tumor.

Many reports of successful treatment of renal tumors with percutaneous radiofrequency ablation (RFA) have been published (77–85). However, real-time monitoring of RFA is not possible with either computerized tomography (CT) or ultrasonography since the thermal ablation zone is not visible with these imaging modalities. RFA can be monitored with MRI

[86,87] but with limitations. Radiofrequency energy has to be interrupted during MRI due to the significant interference it causes otherwise. For example, the temperature-sensitive very short TR/TE gradient echo sequences are typically not suitable for detailed visualization of retroperitoneal anatomy.

Specific to MRI-guided RFA in the kidney, the first report was an *in vivo* study in porcine kidney (88). The procedures were performed in a 0.2T open magnet and demonstrated the suitability of MRI for guiding needle placement, and the benefit of its inherent soft-tissue sensitivity where the electrode could be placed and the thermal lesion observed. Clinical studies of MRI-guided RFA in the kidney subsequently reported the safety and efficacy of the procedure (89,90) in tumors less than 4 cm in diameter. No recurrences at 25 months post-procedure were reported.

Overall RFA has been shown to be a feasible therapeutic modality for kidney lesions whether under MRI, CT or US guidance (91). While RFA is more routinely performed under CT guidance, many practices still turn to MRI for the assessment and long-term follow-up of the treated patient (92–94).

MRI-guided Percutaneous Cryotherapy of Renal Tumors

While RFA may require the need to perform multiple overlapping ablations of larger tumors, with percutaneous cryoablation, larger tumors can be treated simultaneously with the placement of multiple applicators [95,96]. Evidence suggests that renal tumors are more likely to be treated in one session with cryoablation compared to RFA [97]. Lower doses of medications are required for intravenous conscious sedation suggesting that percutaneous cryoablation of renal tumors is associated with less intraprocedural pain than with percutaneous RFA [98]. Ultrasound monitoring of cryoablation is limited by an inability to image the entire iceball due to acoustic shadowing from the edge closest to the ultrasonography probe [99]. Cryoablation of renal tumors can be monitored with CT since the iceball is readily apparent as a hypo-attenuating structure in the renal parenchyma [95,96,99–104]. However, there are two main limitations. One is that the portion of the iceball in the perinephric fat, a hyper-attenuating region, only provides a modest contrast to noise ratio [99–101] compared to surrounding fat, and the ablation zone edge is not clearly demarcated in fatty tissue (Figure 10a). This limits its use for real-time monitoring of the effect of ablation on adjacent critical structures such as bowel, ureter, pancreas, and adrenal gland. Another is that the streak artifact created by the applicators with CT imaging can interfere with iceball visibility (Figure 10b).

Since the initial clinical reports of MRI-guided percutaneous cryoablation of renal tumors [99,101] in 2001, several investigators have shown the feasibility and safety of the procedure [107–114], all demonstrating the advantages of MRI monitoring during percutaneous cryoablation procedures.

MRI depicts the ice ball as a signal void region with high contrast to noise ratio compared to surrounding tissues, with sharp edge definition in multiple planes, and with minimal applicator artifact (Figure 11). Ice ball volume on intraprocedural MRI correlates well with volume of cryonecrosis on post-procedural MRI [114]. Since the ice ball is well depicted on all pulse sequences, the ablation can be monitored using pulse sequences that best display tumor or adjacent critical structures [112]. If images demonstrate incomplete coverage of tumor, additional applicators may be placed to improve coverage [112, 113]. On the other hand, if the ice ball edge approaches adjacent critical structures, the freezing can be stopped [112]. Applicators can be controlled individually. Additional maneuvers to reduce risk of injury to surrounding bowel such as water instillation described for CT-guided ablations [115] can also be performed during MRI-guided cryoablations [112]. A noninvasive method

of external manual displacement of bowel during MRI-guided cryoablation of renal tumors has also been described; a maneuver unique to cryoablation procedures performed in an open-configuration interventional MRI unit [116].

Limitations of MRI-guided cryoablation include the high cost of MRI units and their limited availability, generally long procedure times, smaller gantry sizes compared to CT scanners, and that the inability to detect segment changes of cardiac ischemia on an EKG in the magnetic environment during procedures.

In summary, image-guided percutaneous ablative therapies have the potential to replace conventional surgical treatment of small renal cell carcinoma. Compared to other image-guided ablative therapies, with its vast advantages and minimal limitations, MRI-guided percutaneous cryoablation is well poised to play an important role in the management of renal tumors.

The future

Recent developments in MRI imaging paralleling those in computer-assisted surgery have set up an ideal environment for MR-compatible robotic systems and manipulators. Materials used in mechatronic devices inside the magnet should ideally have a magnetic susceptibility similar to that of human tissue and be electrical insulators to avoid image distortion. Although image quality is reduced due to reduction in static field strength, interventional open-bore magnets have less spatial constraints. On the other hand, closed MR scanners can impose severe constraints on procedural manipulations, despite their imaging advantage of higher field strengths. New wide and short-bore 1.5T magnets (Espree, Siemens, Germany) will expand the utilization of interventional MRI. Emerging use of 3T magnets for interventions will bring about improved monitoring of thermal therapies. Much research is underway evaluating material selection, position detection sensors, different actuation models and techniques, and design strategies (117). Once the engineering hurdle is overcome, systems must then undergo clinical validation before introduction into the commercial realm.

Summary

MRI has become part of routine care in many places around the world, for tumor detection, localization and staging. In the genitourinary tract, MRI-guidance is playing an increasing role in minimally invasive procedures for confirmation of tumor pathology, and both for tumor treatment and treatment monitoring. It offers inherent ability for tumor detection and biopsy guidance, and currently, MR-guided ablative therapies are an increasing and real alternative to more invasive surgical options. As the capabilities of MRI expand and newer imaging modalities become more accessible (PET imaging, for example), the need for non-rigid registration of multiple modalities will be necessary. A combination of functional imaging and high-resolution tumor detail in the genitourinary tract, in a patient-specific treatment environment, should increase demand and the use of semi-invasive or non-invasive technology. Clearly, the pressure is on to provide MR-compatible devices and methodology that easily integrates with imaging and is supportive of patients' clinical needs.

Acknowledgments

This work was supported in part by NIH grant U41RR019703.

References

1. Stewart AJ, Viswanathan AN. Current controversies in high-dose-rate versus low-dose-rate brachytherapy for cervical cancer. Cancer. 2006 Sep 1; 107(5):908–915. [PubMed: 16874815]
2. Stewart EA. Uterine Fibroids. Lancet. 2001; 357:293–298. [PubMed: 11214143]
3. Ravina J, Herbreteau D, Ciraru-Vigneron N, et al. Arterial embolisation to treat uterine myomata. Lancet. 1995; 346:671–672. [PubMed: 7544859]
4. Lynn JG, Zwemer RL, Chick AJ, et al. A new method for the generation and use of focused ultrasound in experimental biology. JGen Physiol. 1942; 26:179–193. [PubMed: 19873337]
5. Fry WJ, Barnard JW, Fry FJ. Ultrasonically produced localized selective lesions in the central nervous system. AM J Phys Med. 1955; 34:413–423. [PubMed: 14376518]
6. Lele PP. A simple method for production of trackless focal lesions with focused ultrasound: physical factors. J Physiol. 1962; 160:494–512. [PubMed: 14463953]
7. Heimburger RF. Ultrasound augmentation of central nervous system tumor therapy. Indiana Med. 1995; 78:469–476. [PubMed: 4020091]
8. Gelet A, Chapelon JY, Bouvier R, et al. Local control of prostate cancer by transrectal high intensity focused ultrasound therapy: preliminary results. J Urol. 1999; 161:156–162. [PubMed: 10037389]
9. Paterson RF, Barret E, Siqueira TM Jr, et al. Laparoscopic partial kidney ablation with high intensity focused ultrasound. J Urol. 2003; 169(1):347–351. [PubMed: 12478187]
10. Yang R, Sanghvi NT, Rescorla FJ, et al. Extracorporeal liver ablation using sonography-guided high-intensity focused ultrasound. Invest Radiol. 1992; 27(10):796–803. [PubMed: 1399435]
11. Watkin NA, Morris SB, Rivens IH, et al. A feasibility study for the non-invasive treatment of superficial bladder tumours with focused ultrasound. Br J Urol. 1996; 78(5):715–721. [PubMed: 8976766]
12. Lizzi FL, Deng CX, Lee P, et al. A comparison of ultrasonic beams for thermal treatment of ocular tumors. Eur J Ultrasound. 1999; 9(1):71–78. [PubMed: 10099168]
13. Ishihara Y, Calderon A, Watanabe H, et al. A precise and fast temperature mapping using water proton chemical shift. Magn Reson Med. 1995; 34(6):814–823. [PubMed: 8598808]
14. Hynynen K, Vykhodtseva NI, Chung AH, et al. Thermal effects of focused ultrasound on the brain: determination with MR imaging. Radiology. 1997; 204(1):247–253. [PubMed: 9205255]
15. Chung AH, Jolesz FA, Hynynen K. Thermal dosimetry of a focused ultrasound beam in vivo by magnetic resonance imaging. Med Phys. 1999; 26(9):2017–2026. [PubMed: 10505893]
16. McDannold N, Tempany CM, Fennessy FM, et al. Uterine leiomyomas: MR imaging-based thermometry and thermal dosimetry during focused ultrasound thermal ablation. Radiology. 2006; 240(1):263–272. [PubMed: 16793983]
17. Chung AH, Hynynen K, Colucci V, et al. Optimization of spoiled gradient-echo phase imaging for in vivo localization of focused ultrasound beam. Magn Reson Med. 1996; 36(5):745–752. [PubMed: 8916025]
18. Leon-Villapalos J, Kaniorou-Larai M, Dziewulski P. Full thickness abdominal burn following magnetic resonance guided focused ultrasound therapy. Burns. 2005; 31(8):1054–1055. [PubMed: 15970389]
19. Tempany CM, Stewart EA, McDannold N, et al. MR imaging-guided focused ultrasound surgery of uterine leiomyomas: a feasibility study. Radiology. 2003; 226(3):897–905. [PubMed: 12616023]
20. Stewart EA, Gedroyc WM, Tempany CM, et al. Focused ultrasound treatment of uterine fibroid tumors: safety and feasibility of a noninvasive thermoablative technique. Am J Obstet Gynecol. 2003; 189(1):48–54. [PubMed: 12861137]
21. Stewart EA, Gostout B, Rabinovici J, et al. Sustained relief of leiomyoma symptoms by using focused ultrasound surgery. Obstet Gynecol. 2007 Aug; 110(2 Pt 1):279–287. [PubMed: 17666601]
22. Fennessy FM, Tempany C, McDannold N, et al. Uterine leiomyomas: MR imaging-guided focused ultrasound surgery--results of different treatment protocols. Radiology. 2007 Jun; 243(3):885–893. [PubMed: 17446521]

23. Morrison PR, Silverman SG, Tuncali K, Tatli S. MRI Guided Cryotherapy. Review. JMRI. 2007 In Press.
24. Sewell PE, Arriola RM, Robinette L, Cowan BD. Real-time I-MR-imaging-guided cryoablation of uterine fibroids. J Vasc Interv Radiol. 2001; 12(7):891–893. [PubMed: 11435548]
25. Cowan BD, Sewell PE, Howard JC, et al. Interventional magnetic resonance imaging cryotherapy of uterine fibroid tumors: preliminary observation. Am J Obstet Gynecol. 2002 Jun; 186(6):1183–1187. [PubMed: 12066095]
26. Dohi M, Harada J, Mogami T, Fukuda K, Kobayashi S, Yasuda M. MR-guided transvaginal cryotherapy of uterine fibroids with a horizontal open MRI system: initial experience. Radiat Med. 2004; 22(6):391–397. [PubMed: 15648454]
27. Sakuhara Y, Shimizu T, Kodama Y, Sawada A, Endo H, Abo D, Hasegawa T, Miyasaka K. Magnetic resonance-guided percutaneous cryoablation of uterine fibroids: early clinical experiences. Cardiovasc Intervent Radiol. 2006 Jul-Aug; 29(4):552–558. [PubMed: 16532267]
28. Amercian Cancer Society. Cancer facts and figures 2007. Atlanta, Ga: American Cancer Society; 2006. Publication no. 500807
29. Cancer Facts and Figures. Atlanta: American Cancer Society; 2008.
30. Lee F, Gray JM, McLeary RD, et al. Prostatic evaluation by transrectal sonography: criteria for diagnosis of early carcinoma. Radiology. 1986; 158:91–95. [PubMed: 3510031]
31. Terris MK. Sensitivity and specificity of sextant biopsies in the detection of prostate cancer; preliminary report. Urology. 1999; 54:486–489. [PubMed: 10475359]
32. Aus G, Hermansson CG, Hugosson J, Pederson KV. Transrectal ultrasound examination of the prostate: complications and acceptance by patients. Br J Urol. 1993; 71:457–459. [PubMed: 8499990]
33. Collins GN, Lloyd SN, Hehir M, McKelvie GB. Multiple transrectal ultrasound-guided prostatic biopsies: true morbidity and patient acceptance. Br J Urol. 1993; 71:460–463. [PubMed: 8499991]
34. Rodriguez LV, Terris MK. Risks and complications of transrectal ultrasound guided prostate needle biopsy: a prospective review of the literature. J Urol. 1998; 160:2115–2120. [PubMed: 9817335]
35. Rifkin MD, Zerhouni EA, Gatsonis CA, et al. Comparison of magnetic resonance imaging and ultrasonography in staging early prostate cancer: results of a multi-institutional cooperative trial. N Engl J Med. 1990; 323:621–626. [PubMed: 2200965]
36. Schnall MD, Pollack HM. Magnetic resonance imaging of the prostate gland. Urol Radiol. 1990; 12(2):109–114. [PubMed: 1700526]
37. Cornud F, Flam T, Chauveinc L, et al. Extraprostatic spread of clinically localized prostate cancer: factors predictive of pT3 tumor and of positive endorectal MR imaging examination results. Radiology. 2002 Jul; 224(1):203–210. [PubMed: 12091684]
38. Outwater EK, Petersen RO, Siegelman ES, et al. Prostate carcinoma: assessment of diagnostic criteria for capsular penetration on endorectal coil MR images. Radiology. 1994 Nov; 193(2):333–339. [PubMed: 7972739]
39. Mullerad M, Hricak H, Kuroiwa K, et al. Comparison of endorectal magnetic resonance imaging, guided prostate biopsy and digital rectal examination in the preoperative anatomical localization of prostate cancer. J Urol. 2005; 174:2158–2163. [PubMed: 16280755]
40. Perrotti M, Han KR, Epstein RE, et al. Prospective evaluation of endorectal magnetic resonance imaging to detect tumor foci in men with prior negative prostatic biopsy: a pilot study. J Urol. 1999; 162:1314–1317. [PubMed: 10492187]
41. Hata N, Morrison PR, Kettenbach J, Kikinis R, Jolesz FA. Computer-assisted intra-operative MRI monitoring of interstitial laser therapy in the brain: a case report. SPIE J Biomed Optics. 1998; 3:302–311.
42. Gering, D.; Nabavi, A.; Kikinis, R., et al. Medical Image Computing and Computer-Assisted Intervention (MICCAI). Cambridge, England: 1999 September 22. An integrated visualization system for surgical planning and guidance using image fusion and interventional imaging.
43. D'Amico AV, Cormack R, Tempany CM, et al. Real-time magnetic resonance image-guided interstitial brachytherapy in the treatment of select patients with clinically localized prostate cancer. Int J Radiat Oncol Biol Phys. 1998; 42:507–515. [PubMed: 9806508]

44. Hata N, Jinzaki M, Kacher D, et al. MR Imaging-guided prostate biopsy with surgical navigation software; device validation and feasibility. Radiology. 2001; 220:263–268. [PubMed: 11426008]
45. Susil RC, Camphausen K, Choyke P, et al. System for prostate brachytherapy and biopsy in a standard 1.5 T MRI scanner. Magn Reson Med. 2004; 52(3):683–687. [PubMed: 15334592]
46. Susil RC, Menard C, Kreiger A, et al. Transrectal prostate biopsy and fiducial marker placement in a standard 1.5T magnetic resonance imaging scanner. J Urol. 2006 Jan; 175(1):113–120. [PubMed: 16406885]
47. Beyersdorff D, Winkel A, Hamm B, et al. MR imaging-guided prostate biopsy with a closed MR unit at 1.5 T: initial results. Radiology. 2005; 234(2):576–581. [PubMed: 15616117]
48. Kreiger A, Susil RC, Menard C, et al. Design of a novel MRI compatible manipulator for image guided prostate interventions. IEEE Trans Biomed Eng. 2005; 52(2):306–313. [PubMed: 15709668]
49. Singh AK, Kreiger A, Lattouf JB. Patient selection determines the prostate cancer yield of dynamic contrast-enhanced magnetic resonance imaging-guided transrectal biopsies in a closed 3-Tesla scanner. BJU Int. 2007 Oct 8. (Epub).
50. DiMaio SP, Pieper S, Chinzei K, et al. Robot-assisted needle placement in open MRI: system architecture, integration and validation. Comput Aided Surg. 2007 Jan; 12(1):15–24. [PubMed: 17364655]
51. Lee WR, Hall MC, McQuellon RP, et al. A prospective quality-of-life study in men with clinically localized prostate carcinoma treated with radical prostatectomy, external beam radiotherapy, or interstitial brachytherapy. Int J Radiat Oncol Biol Phys. 2001; 51(3):614–623. [PubMed: 11597800]
52. Zelefsky MJ, Yamada Y, Marion C, et al. Improved conformality and decreased toxicity with intraoperative computer-optimized transperineal ultrasound-guided prostate brachytherapy. Int J Radiat Oncol Biol Phys. 2003 Mar 15; 55(4):956–963. [PubMed: 12605973]
53. Kooy HM, Cormack RA, Mathiowitz RV, et al. A software system for interventional magnetic resonance image-guided prostate brachytherapy. Comput Aided Surg. 2000; 5(6):401–413. [PubMed: 11295853]
54. D'Amico AV, Cormack R, Kumar S, et al. Real-time magnetic resonance imaging-guided brachytherapy in the treatment of selected patients with clinically localized prostate cancer. J Endourol. 2000; 14:367–370. [PubMed: 10910153]
55. Albert M, Tempany CM, Schultz D, et al. Late genitourinary and gastrointestinal toxicity after magnetic resonance image-guided prostate brachytherapy with or without neoadjuvant external beam radiation therapy. Cancer. 2003 Sep 1; 98(5):949–954. [PubMed: 12942561]
56. Nguyen PL, Chen MH, D'Amico AV, et al. Magnetic resonance image-guided salvage brachytherapy after radiation in select men who initially presented with favorable-risk prostate cancer: a prospective phase 2 study. Cancer. 2007 Oct 1; 110(7):1485–1492. [PubMed: 17701957]
57. D'Amico AV, Moul J, Carroll PR, et al. Cancer-specific mortality after surgery or radiation for patients with clinically localized prostate cancer managed during the prostate-specific antigen era. J Clin Oncol. 2003; 21(11):2163–2172. [PubMed: 12775742]
58. Sylvester JE, Grimm PD, Blasko JC, et al. 5-Year biochemical relapse free survival in clinical Stage T1-T3 prostate cancer following combined external beam radiotherapy and brachytherapy; Seattle experience. Int J Radiat Oncol Biol Phys. 2007; 67(1):57–64. [PubMed: 17084544]
59. Lawton CA, DeSilvo M, Lee WR, et al. Results of a phase II trial of transrectal ultrasound-guided permanent radioactive implantation of the prostate for definitive management of localized adenocarcinoma of the prostate (radiation therapy oncology group 98–05. Int J Radiat Oncol Biol Phys. 2007 Jan 1; 67(1):39–47. [PubMed: 17084551]
60. Chinzei K, Miller K. Towards MRI guided surgical manipulator. Med Sci Monit. 2001; 7:153–163. [PubMed: 11208513]
61. Poissonier L, Chapelon JY, Rouviere O, et al. Control of prostate cancer by transrectal HIFU in 227 patients. Eur Urol. 2007 Feb; 51(2):381–387. [PubMed: 16857310]
62. Uchida T, Ohkusa H, Nagata Y, Hyodo T, Satoh T, Irie A. Treatment of localized prostate cancer using high-intensity focused ultrasound. BJU Int. 2006; 97(1):56–61. [PubMed: 16336329]

63. Ficarra V, Antoniolli SZ, Novara G, et al. Short-term outcome after high-intensity focused ultrasound in the treatment of patients with high-risk prostate cancer. BJU Int. 2006 Dec; 98(6): 1193–1198. [PubMed: 17125477]
64. Smith NB, Buchanan MT, Hynynen K. Transrectal ultrasound applicator for prostate heating monitored using MRI thermometry. Int J Radiat Oncol Biol Phys. 1999; 43(1):217–225. [PubMed: 9989529]
65. Sokka SD, King RL, McDannold NJ, Hynynen K. Design and evaluation of a linear intracavitary ultrasound phased array for MRI-guided prostate ablative therapies. Proceedings of the Ultrasonics Symposium. 2000:1435–1438.
66. Nau WH, Diederich CJ, Ross AB, et al. MRI-guided interstitial ultrasound thermal therapy of the prostate: a feasibility study in the canine model. Med Phys. 2005; 32(3):733–743. [PubMed: 15839345]
67. Pauly KB, Diedrich CJ, Rieke V, et al. Magnetic resonance-guided high-intensity ultrasound ablation of the prostate. Top Magn Reson Imaging. 2006; 17(3):195–207. [PubMed: 17414077]
68. Diederich CJ, Nau WH, Ross AB, Tyreus PD, Butts K, Rieke V, et al. Catheter-based ultrasound applicators for selective thermal ablation: progress towards MRI-guided applications in prostate. Int J Hyperthermia. 2004; 20(7):739–756. [PubMed: 15675669]
69. Diederich CJ, Stafford RJ, Nau WH, Burdette EC, Price RE, Hazle JD. Transurethral ultrasound applicators with directional heating patterns for prostate thermal therapy: in vivo evaluation using magnetic resonance thermometry. Medical Physics. 2004; 31(2):405–413. [PubMed: 15000627]
70. Hazle JD, Diederich CJ, Kangasniemi M, Price RE, Olsson LE, Stafford RJ. MRI-guided thermal therapy of transplanted tumors in the canine prostate using a directional transurethral ultrasound applicator. J Magn Reson Imaging. 2002; 15(4):409–417. [PubMed: 11948830]
71. Chopra R, Burtnyk M, Haider MA, Bronskill MJ. Method for MRI-guided conformal thermal therapy of prostate with planar transurethral ultrasound heating applicators. Phys Med Biol. 2005; 50(21):4957–4975. [PubMed: 16237234]
72. Ross AB, Diederich CJ, Nau WH, Gill H, Bouley DM, Daniel B, et al. Highly Directional Transurethral Ultrasound Applicators with Rotational Control for MRI Guided Prostatic Thermal Therapy. Physics in Medicine and Biology. 2004; 49(1):189–204. [PubMed: 15083666]
73. Ross AB, Diederich CJ, Nau WH, Rieke V, Butts RK, Sommer G, et al. Curvilinear transurethral ultrasound applicator for selective prostate thermal therapy. Med Phys. 2005; 32(6):1555–1565. [PubMed: 16013714]
74. Godley PA, Ataga KI. Renal cell carcinoma. Curr Opin Oncol. 2000; 12:260–264. [PubMed: 10841199]
75. Chow WH, Devesa SS, Warren JL, Fraumeni JF. Rising incidence of renal cell cancer in the United States. JAMA. 1999; 281:1628–1631. [PubMed: 10235157]
76. Link RE, Permpongkosol S, Gupta A, Jarrett TW, Solomon SB, Kavoussi LR. Cost analysis of open, laparoscopic, and percutaneous treatment options for nephron-sparing surgery. J Endourol. 2006; 20:782–789. [PubMed: 17094755]
77. Gervais DA, McGovern FJ, Wood BJ, Goldberg SN, McDougal WS, Mueller PR. Radio-frequency ablation of renal cell carcinoma: early clinical experience. Radiology. 2000; 217:665–672. [PubMed: 11110926]
78. Ogan K, Jacomides L, Dolmatch BL, et al. Percutaneous radiofrequency ablation of renal tumors: technique, limitations, and morbidity. Urology. 2002; 60:954–958. [PubMed: 12475648]
79. Farrell MA, Charboneau WJ, DiMarco DS, et al. Imaging-guided radiofrequency ablation of solid renal tumors. AJR. 2003; 180:1509–1513. [PubMed: 12760910]
80. Mayo-Smith WW, Dupuy DE, Parikh PM, Pezzullo JA, Cronan JJ. Imaging-guided percutaneous radiofrequency ablation of solid renal masses: technique and outcomes of 38 treatment sessions in 32 consecutive patients. AJR. 2003; 180:1503–1508. [PubMed: 12760909]
81. Roy-Choudhury SH, Cast JE, Cooksey G, Puri S, Breen DJ. Early experience with percutaneous radiofrequency ablation of small solid renal masses. AJR. 2003; 180:1055–1061. [PubMed: 12646454]

82. Su LM, Jarrett TW, Chan DYS, Kavoussi LR, Solomon SB. Percutaneous computed tomography-guided radiofrequency ablation of renal masses in high surgical risk patients: preliminary results. Urology. 2003; 61:26–33. [PubMed: 12657358]
83. Zagoria RJ, Hawkins AD, Clark PE, et al. Percutaneous CT-guided radiofrequency ablation of renal neoplasms: factors influencing success. AJR. 2004; 183:201–207. [PubMed: 15208139]
84. Gervais DA, McGovern FJ, Arellano RS, McDougal WS, Mueller PR. Radiofrequency ablation of renal cell carcinoma: part 1, indications, results, and role in patient management over 6-year period and ablation of 100 tumors. AJR. 2005; 185:64–71. [PubMed: 15972400]
85. Varkarakis IM, Allaf ME, Inagaki T, et al. Percutaneous radiofrequency ablation of renal masses: results at a 2-year mean followup. J Urol. 2005; 174:456–460. [PubMed: 16006864]
86. Lewin JS, Connell CF, Duerk JL, et al. Interactive MRI-guided radiofrequency interstitial thermal ablation of abdominal tumors: clinical trial for evaluation of safety and feasibility. JMRI. 1998; 8:40–47. [PubMed: 9500259]
87. Lewin JS, Nour SG, Connell CF, et al. Phase II clinical trial of interactive MR imaging-guided interstitial radiofrequency thermal ablation of primary kidney tumors: initial experience. Radiology. 2004; 232:835–845. [PubMed: 15333798]
88. Merkle EM, Shonk JR, Duerk JL, Jacobs GH, Lewin JS. MR-guided RF thermal ablation of the kidney in a porcine model. AJR Am J Roentgenol. 1999 Sep; 173(3):645–651. [PubMed: 10470895]
89. Lewin JS, Nour SG, Connell CF, Sulman A, Duerk JL, Resnick MI, Haaga JR. Phase II clinical trial of interactive MR imaging-guided interstitial radiofrequency thermal ablation of primary kidney tumors: initial experience. Radiology. 2004 Sep; 232(3):835–845. [PubMed: 15333798]
90. Boss A, Clasen S, Kuczyk M, Anastasiadis A, Schmidt D, Graf H, Schick F, Claussen CD, Pereira PL. Magnetic resonance-guided percutaneous radiofrequency ablation of renal cell carcinomas: a pilot clinical study. Invest Radiol. 2005 Sep; 40(9):583–590. [PubMed: 16118551]
91. Boss A, Clasen S, Kuczyk M, Schick F, Pereira PL. Image-guided radiofrequency ablation of renal cell carcinoma. Eur Radiol. 2007 Mar; 17(3):725–733. [PubMed: 17021704]
92. Merkle EM, Nour SG, Lewin JS. MR imaging follow-up after percutaneous radiofrequency ablation of renal cell carcinoma: findings in 18 patients during first 6 months. Radiology. 2005 Jun; 235(3):1065–1071. [PubMed: 15914485]
93. Memarsadeghi M, Schmook T, Remzi M, Weber M, Potscher G, Lammer J, Kettenbach J. Percutaneous radiofrequency ablation of renal tumors: midterm results in 16 patients. Eur J Radiol. 2006 Aug; 59(2):183–189. [PubMed: 16725292]
94. Kawamoto S, Permpongkosol S, Bluemke DA, Fishman EK, Solomon SB. Sequential changes after radiofrequency ablation and cryoablation of renal neoplasms: role of CT and MR imaging. Radiographics. 2007 Mar–Apr; 27(2):343–355. [PubMed: 17374857]
95. Atwell TD, Farrell MA, Callstrom MR, et al. Percutaneous cryoablation of 40 solid renal tumors with US guidance and CT monitoring: initial experience. Radiology. 2007; 243:276–283. [PubMed: 17329689]
96. Atwell TD, Farrell MA, Callstrom MR, et al. Percutaneous cryoablation of large renal masses: technical feasibility and short-term outcome. AJR. 2007; 188:1195–1200. [PubMed: 17449758]
97. Matina SF, Ahrarb K, Cadedduc JA, et al. Residual and recurrent disease following renal energy ablative therapy: a multi-institutional study. J Urol. 2006; 176:1973–1977. [PubMed: 17070224]
98. Allaf ME, Varkarakis IM, Bhayani SB, Inagaki T, Kavoussi LR, Solomon SB. Pain control requirements for percutaneous ablation of renal tumors: cryoablation versus radiofrequency ablation--initial observations. Radiology. 2005; 237:366–370. [PubMed: 16126920]
99. Tacke J, Speetzen R, Heschel I, Hunter DW, Rau G, Gunther RW. Imaging of interstitial cryotherapy--an in vitro comparison of ultrasound, computed tomography, and magnetic resonance imaging. Cryobiology. 1999; 38:250–259. [PubMed: 10328915]
100. Saliken J, McKinnon J, Gray R. CT for monitoring cryotherapy. AJR. 1996; 166:853–855. [PubMed: 8610562]
101. Sandison GA, Loye MP, Rewcastle JC, et al. X-ray CT monitoring of iceball growth and thermal distribution during cryosurgery. Phys Med Biol. 1998; 43:3309–3324. [PubMed: 9832018]

102. Gupta A, Allaf ME, Kavoussi LR, et al. Computerized Tomography Guided Percutaneous Renal Cryoablation With the Patient Under Conscious Sedation: Initial Clinical Experience. J Urol. 2006; 175:447–453. [PubMed: 16406968]

103. Permpongkosol S, Link RE, Kavoussi LR, Solomon SB. Percutaneous computerized tomography guided cryoablation for localized renal cell carcinoma: factors influencing success. J Urol. 2006; 176:1963–1968. [PubMed: 17070219]

104. Littrup PJ, Ahmed A, Aoun HD, et al. CT-guided percutaneous cryotherapy of renal masses. J Vasc Interv Radiol. 2007; 18:383–392. [PubMed: 17377184]

105. Harada J, Dohi M, Mogami T, et al. Initial experience of percutaneous renal cryosurgery under the guidance of a horizontal open MRI system. Radiat Med. 2001; 19:291–296. [PubMed: 11837579]

106. Shingleton WB, Sewell J, Patrick E. Percutaneous renal tumor cryoablation with magnetic resonance imaging guidance. J Urol. 2001; 165:773–776. [PubMed: 11176465]

107. Shingleton WB, Sewell PE. Percutaneous renal cryoablation of renal tumors in patients with von Hippel-Lindau disease. J Urol. 2002; 167:1268–1270. [PubMed: 11832711]

108. Shingleton WB, Sewell PE. Percutaneous cryoablation of renal cell carcinoma in a transplanted kidney. BJU International. 2002; 90:137–138. [PubMed: 12081786]

109. Sewell PE, Howard JC, Shingleton WB, Harrison RB. Interventional magnetic resonance image-guided percutaneous cryoablation of renal tumors. Southern Medical Journal. 2003; 96:708–710. [PubMed: 12940328]

110. Shingleton WB, Sewell PE. Cryoablation of renal tumours in patients with solitary kidneys. BJU International. 2003; 92:237–239. [PubMed: 12887474]

111. Kodama Y, Abo D, Sakuhara Y, et al. MR-guided percutaneous cryoablation for bilateral multiple renal cell carcinoma. Radiat Med. 2005; 23:303–307. [PubMed: 16012408]

112. Silverman SG, Tuncali K, vanSonnenberg E, et al. Renal tumors: MR imaging guided percutaneous cryotherapy--initial experience in 23 patients. Radiology. 2005; 236:716–724. [PubMed: 16040927]

113. Miki K, Shimomura T, Yamada H, et al. Percutaneous cryoablation of renal cell carcinoma guided by horizontal open magnetic resonance imaging. International Journal of Urology. 2006; 13:880–884. [PubMed: 16882047]

114. Silverman SG, Tuncali K, Adams DF, et al. MR imaging-guided percutaneous cryotherapy of liver tumors: initial experience. Radiology. 2000; 217:657–664. [PubMed: 11110925]

115. Farrell MA, Charboneau JW, Callstrom MR, Reading CC, Engen DE, Blute ML. Paranephric water instillation: a technique to prevent bowel injury during percutaneous renal radiofrequency ablation. AJR. 2003; 181:1315–1317. [PubMed: 14573426]

116. Tuncali K, Morrison PR, Tatli S, Silverman SG. MRI-guided percutaneous cryoablation of renal tumors: use of external manual displacement of adjacent bowel loops. European Journal of Radiology. 2006; 59:198–202. [PubMed: 16716551]

117. Elhawary H, Zivanovic A, Davies B, Lamperth M. A review of magnetic resonance imaging compatible manipulators in surgery. Proc Inst Mech Eng [H]. 2006 Apr; 220(3):413–424.

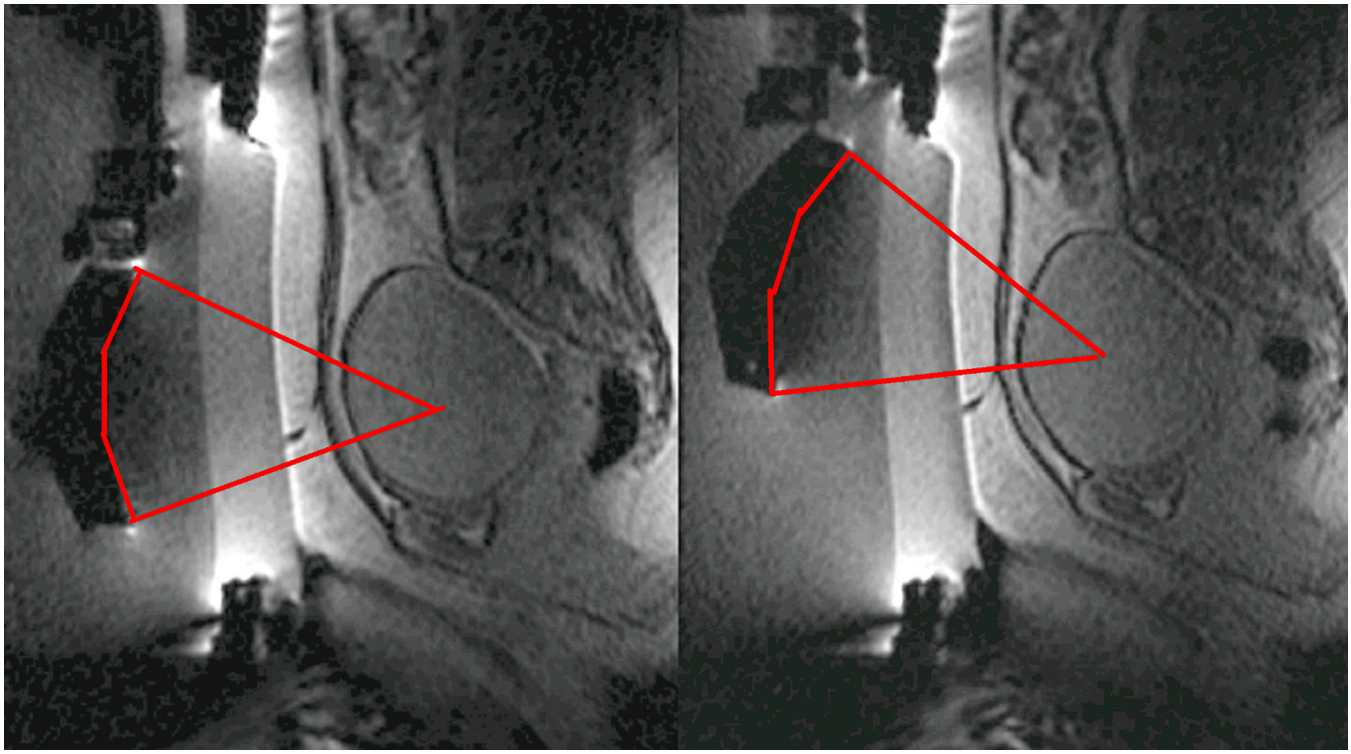

Figure 1.
Linear scar through the subcutaneous tissue lies between the transducer and the fibroid, on the sagittal localizer image on the left. The sagittal localizer image on the right is obtained after tilting the transducer superiorly, without moving the patient, allowing treatment planning that will not course through the anterior abdominal subcutaneous tissue scar. (Reproduced, with permission, from Lippincott Williams and Wilkins. “A review of magnetic resonance imaging-guided focused ultrasound surgery of uterine fibroids", Top Magn Reson Imaging. 2006 Jun;17(3):173-9).

Figure 2.
The sagittal localizer image on the left demonstrates bowel loops coursing between the anterior abdominal wall and the uterine fibroid. After placement of a spacer device (sagittal localizer image on the right) under the anterior abdominal wall, the bowel loops are displaced, allowing for treatment through a larger acoustic window. (Reproduced, with permission, from Lippincott Williams and Wilkins. “A review of magnetic resonance imaging-guided focused ultrasound surgery of uterine fibroids", Top Magn Reson Imaging. 2006 Jun;17(3):173–9).

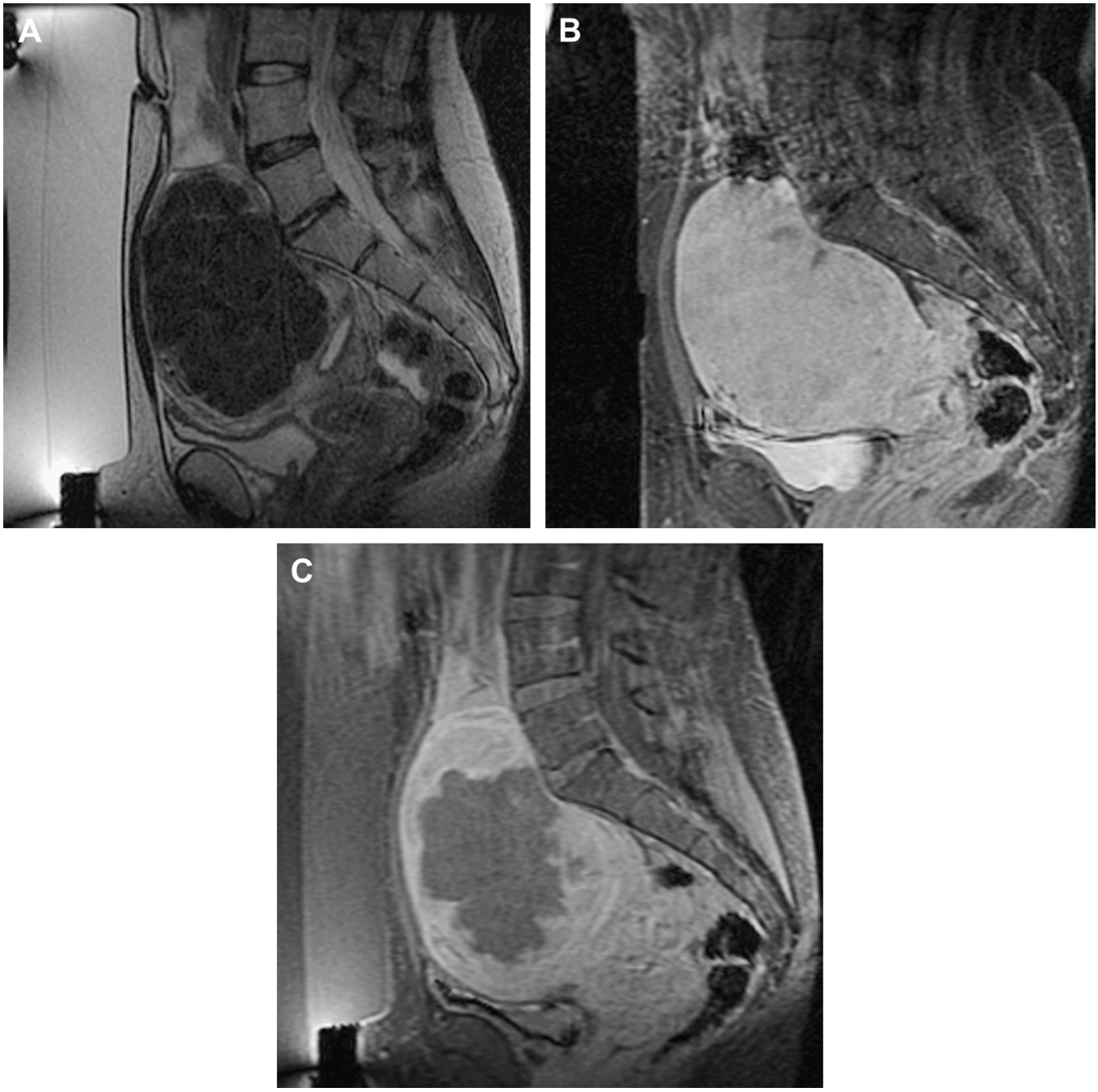

Figure 3.
Imaging of a uterine fibroid pre (A, B)- and post (C)-treatment with MRgFUS. Sagittal T2 weighted image (A), obtained with the patient in the prone position overlying the ultrasound transducer, demonstrates a large solitary uterine fibroid of low signal intensity. Sagittal fast spoiled gradient-recalled-echo sequence (SPGR) post Gadolinium® (B) demonstrates homogenous enhancement of the fibroid. After treatment, sagittal SPGR post Gadolinium® (C) demonstrates a new large non-perfused area within the fibroid, consistent with treatment-induced necrosis.

Figure 4.
Photograph (courtesy of Yusuke Sakuhara, MD, Department of Radiology, Hokkaido University Hospital, Sapporo, Japan) demonstrating the set-up for percutaneous MRI-guided cryotherapy for uterine fibroids in an open horizontal 0.3 T AIRIS II (Hitachi, Tokyo, Japan) scanner.

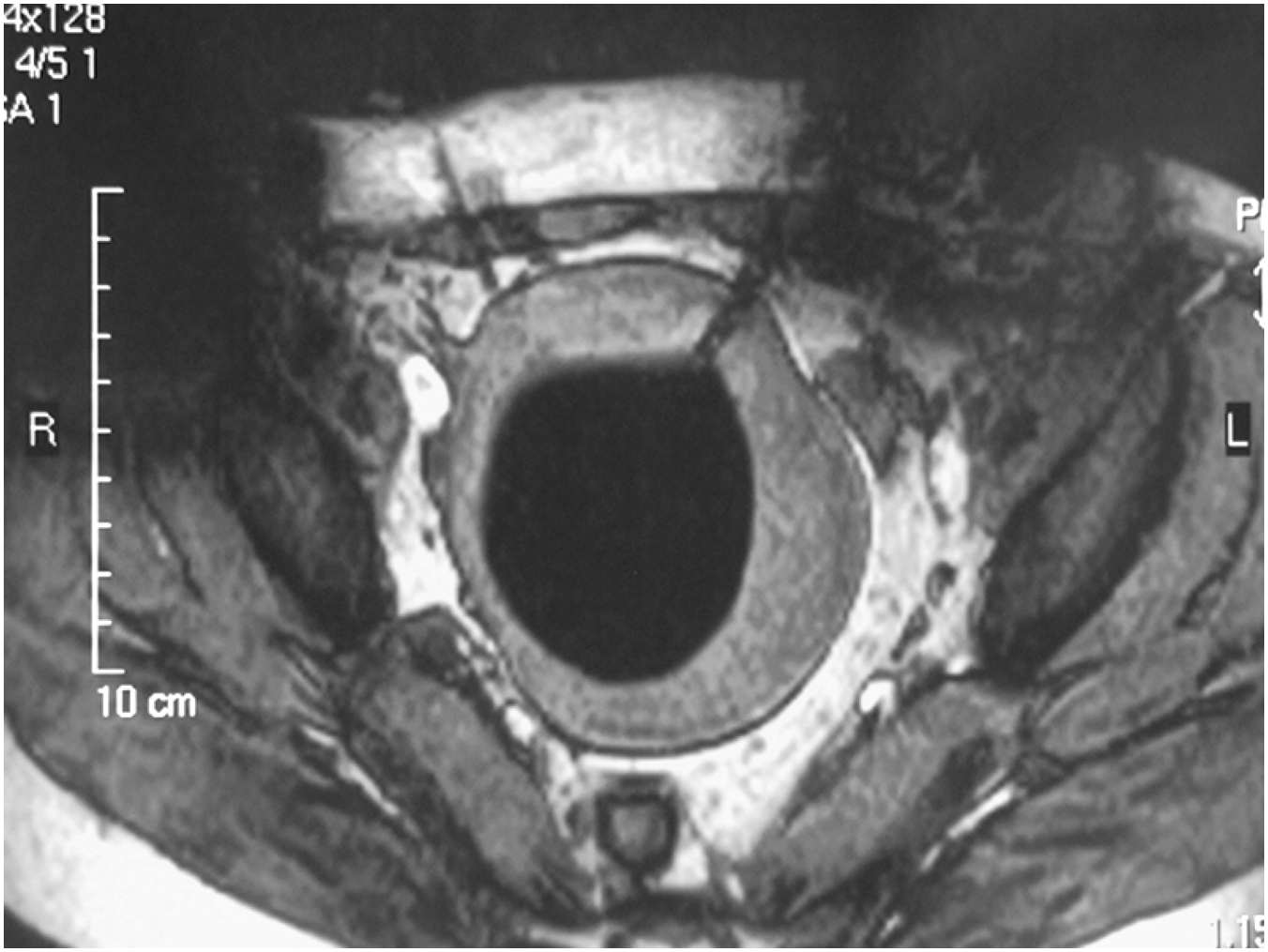

Figure 5.
Axial T2 weighted spin echo sequence demonstrating a probe in the left anterolateral aspect of a uterine fibroid. The diffuse low signal intensity in the fibroid represents the ice-ball. (Image courtesy of Yusuke Sakuhara, MD, Department of Radiology, Hokkaido University Hospital, Sapporo, Japan)

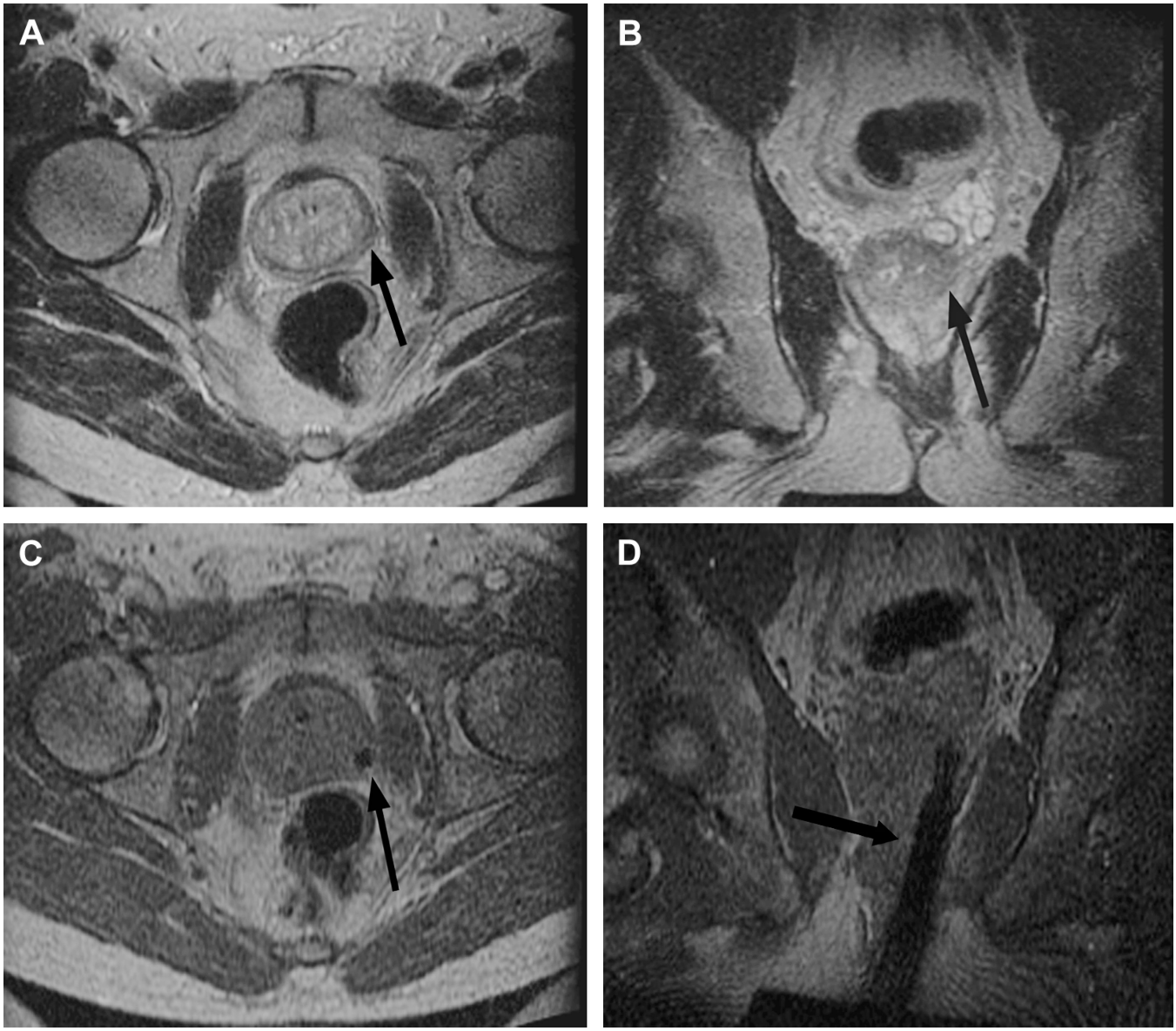

Figure 6.
Imaging before and during MRI-guided prostate biopsy.
Axial (A) and coronal (B) T2 weighted spin echo sequence outline areas to be biopsied. In this example, an area in the left mid gland is demonstrated (arrow), reformatted to the same spatial location as the corresponding real-time axial (C) and coronal images (D) taken during needle insertion. The biopsy needle is seen in cross-section as a circle of low signal intensity (arrow) on the axial gradient echo real-time image (C) and as a longitudinal area of low signal intensity (arrow) on the coronal gradient echo real-time image (D).

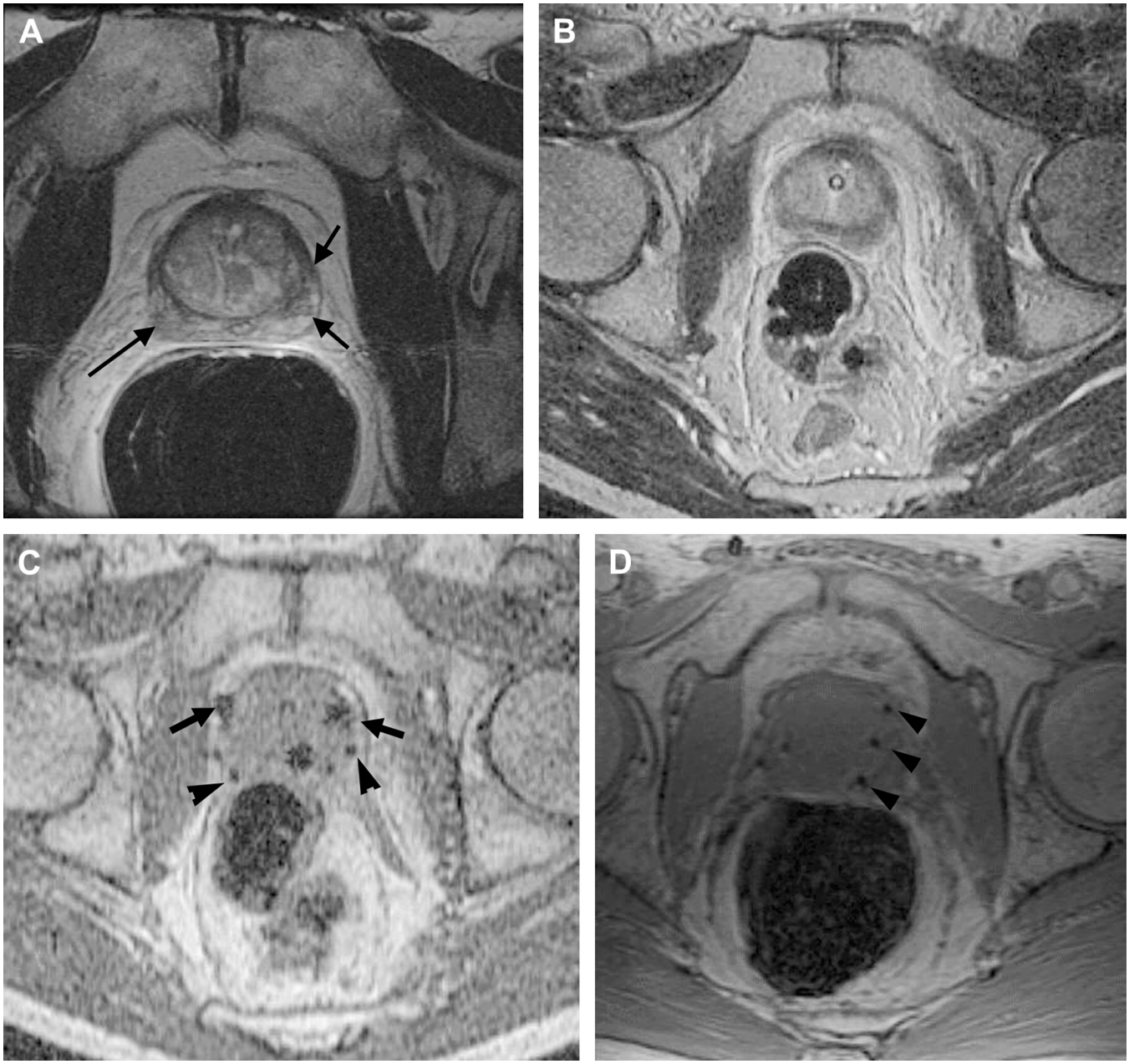

Figure 7.

Pre-, intra-, and post-operative MRI-guided brachytherapy in prostate cancer.

Pre-operative 1.5T (A) axial T2 weighted spin echo image through the prostate base, demonstrating low signal intensity in the peripheral zone (arrows), previously demonstrated to be tumor. Intra-operative 0.5T (B) axial T2 weighted spin echo T2 weighted spin echo image through the same area. Intra-operative axial gradient echo MR images (C) obtained in real-time during needle and seed placement in the prostate base. The larger round areas represent the needles (arrows), prior to deployment, and the small round areas represent the deployed seeds (arrowheads). A post-operative axial SPGR through the prostate base demonstrates multiple round areas of low signal in the peripheral zone (arrowheads), consistent with deployed seeds.

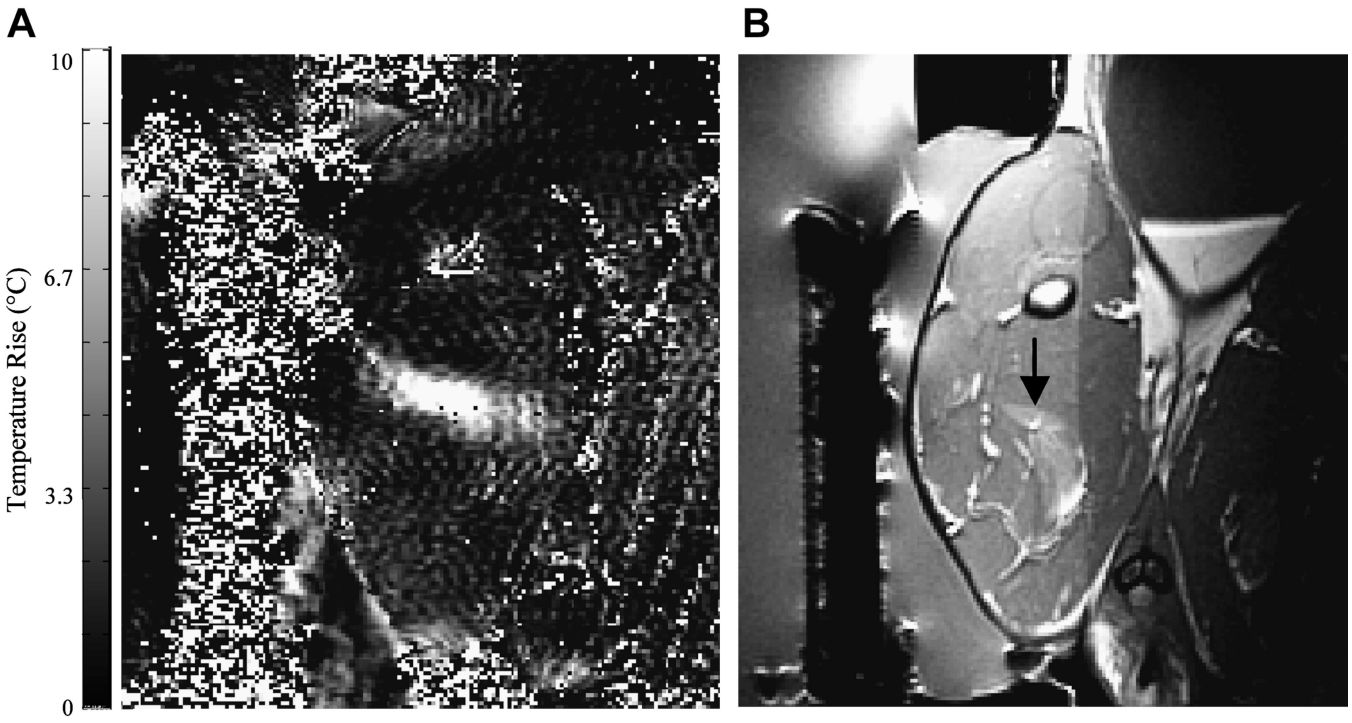

Figure 8.

(a) MRI-based temperature image during a sonication (130 W for 30 seconds) into rabbit thigh muscle during a test of an MRI-compatible transrectal phased array applicator for MRgFUS of prostate (b) The thermal lesion (arrow) seen in T2-weighted imaging. The bright region to the right of the lesion is a tissue fascia layer. Figure reproduced from Sokka SD, Hynynen K. The feasibility of MRI-guided whole prostate ablation with a linear aperiodic intracavitary ultrasound phased array. Phys Med Biol 2000; 45:3373–3383), with permission from the authors and from the publisher (Institute of Physics Publishing, Bristol, UK, Editor: S. Webb).

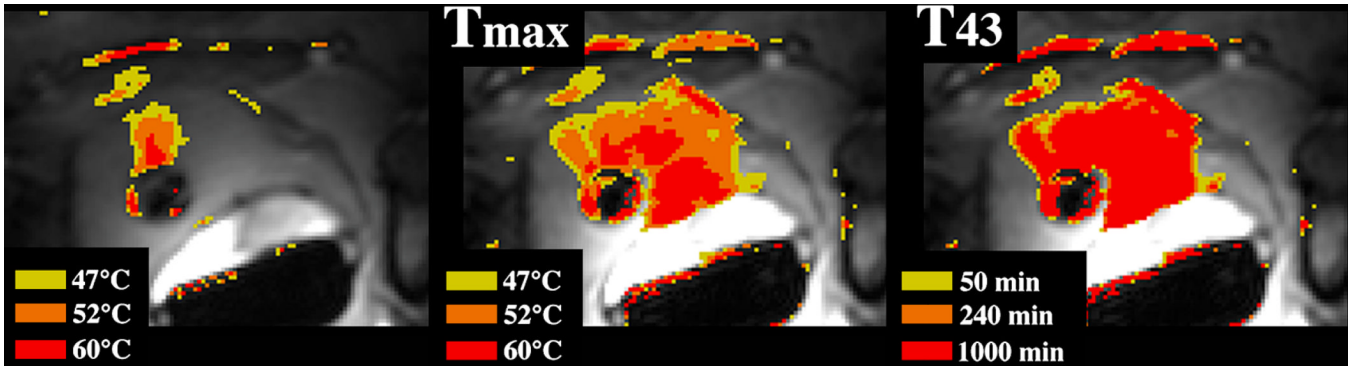

Figure 9.

MRI-guided catheter-based ultrasound thermal therapy of the prostate:
Real-time temperature image (left), maximum temperature image (middle), and thermal dose (right) of the prostate during catheter-based ultrasound thermal therapy. The transurethral catheter, with a rotating curvilinear transducer array, is depicted as the round low signal intensity structure within the prostate gland (69). (Courtesy of Kim Butts Pauly, PhD, Viola Rieke, MD and Graham Sommer, PhD, Stanford University School of Medicine, CA and Chris Diederich, PhD,UCSF, CA).

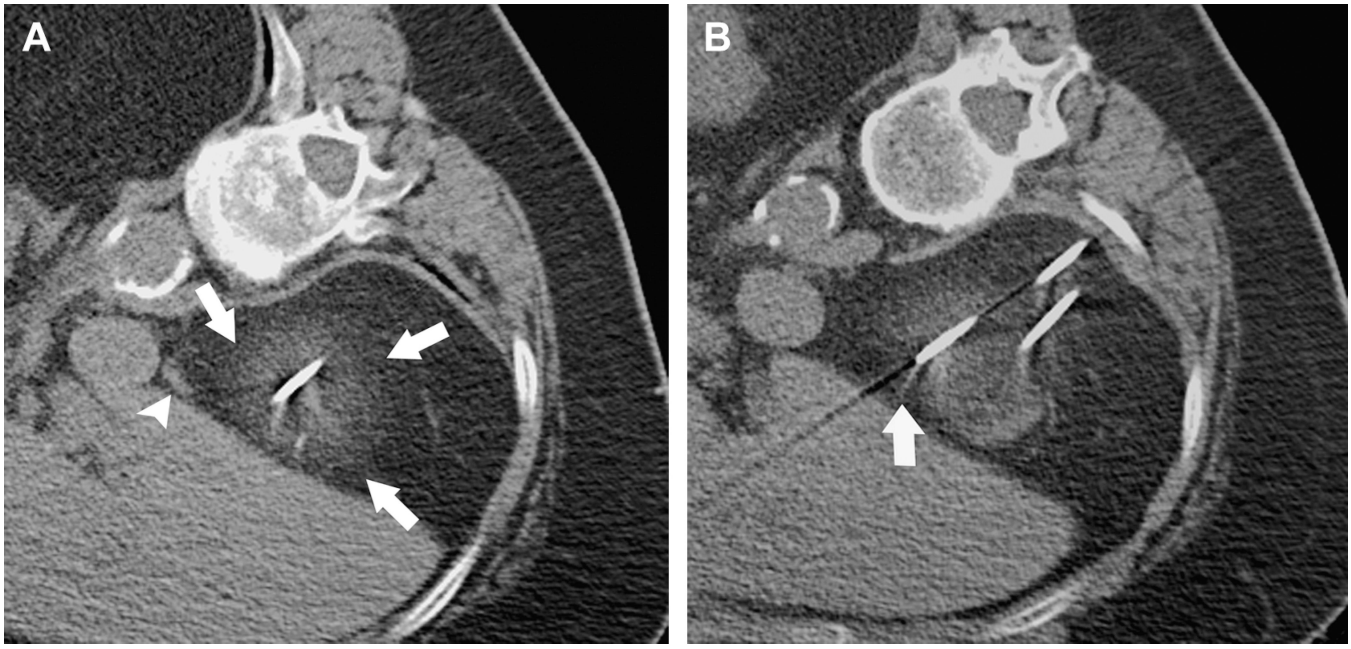

Figure 10.

MRI-guided Percutaneous Cryotherapy of Renal Tumors

77-year-old woman with renal cell carcinoma of the right kidney upper pole. Unenhanced transverse CT images obtained during percutaneous cryoablation performed in the right lateral decubitus position show that (a) low contrast to noise ratio and poor edge definition of ice ball (arrows) in the perinephric fat renders assessment for overlap of ablation zone with adjacent adrenal gland (arrowhead) difficult, and (b) streak artifact from applicator interferes with visualization of portion of the ice ball (arrow).

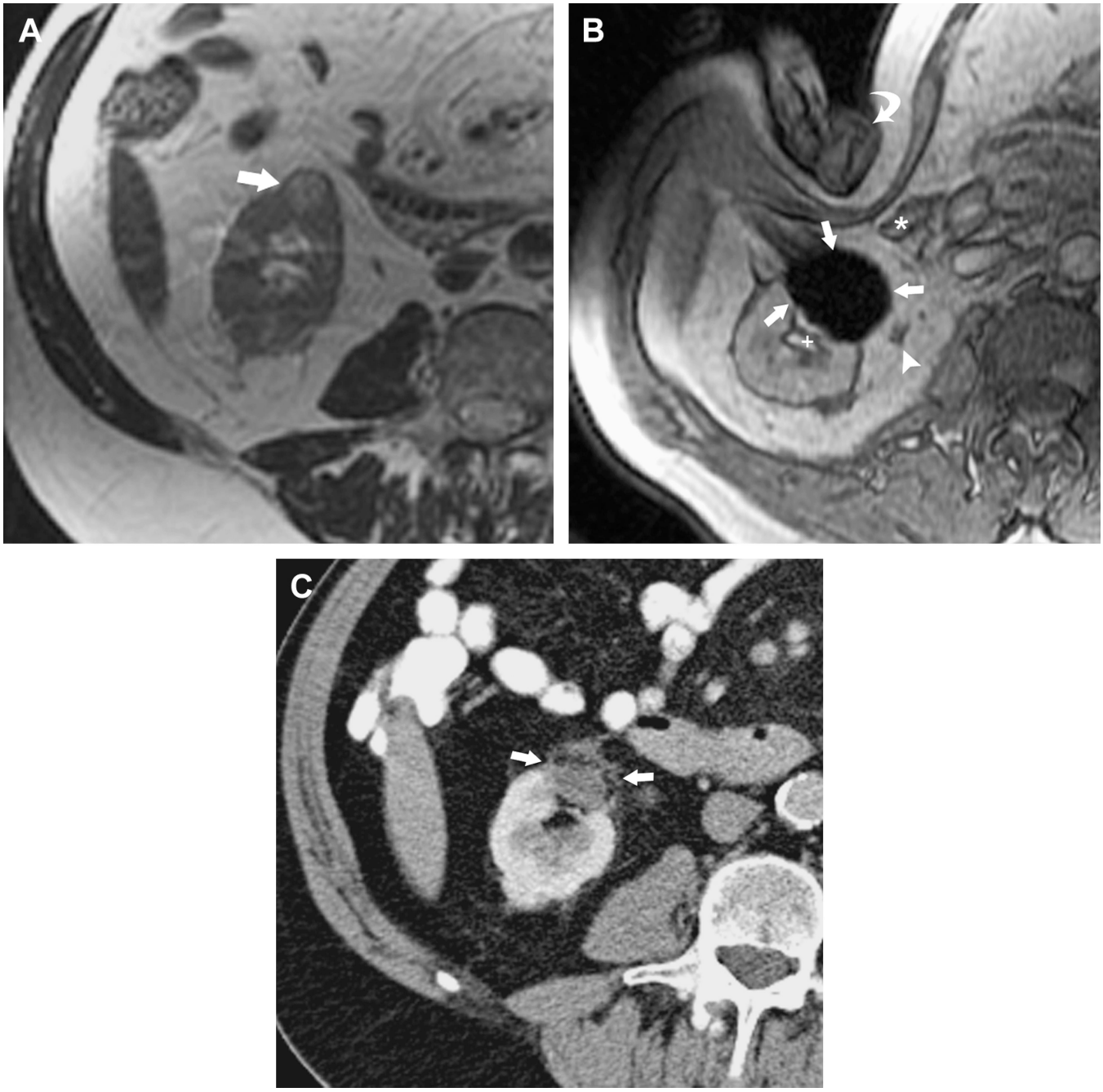

Figure 11.

MRI-guided Percutaneous Cryotherapy of Renal Tumors

70-year-old man with renal cell carcinoma of the right kidney lower pole treated with MRI-guided percutaneous cryoablation. (a) Transverse T2-weighted FRFSE image obtained before treatment in 1.5 T MRI shows a small exophytic renal mass in the lower pole of the right kidney anteriorly (arrow). (b) Intraprocedural transverse gradient echo image obtained in 0.5 T open configuration interventional MRI shows that sharp edge definition of signal void ice ball (arrows) contributes to monitoring of tumor coverage and assessment of proximity to adjacent ureter (arrowhead), renal collecting system (+), and colon (*) which is being displaced by the interventionalist's hand (curved arrow). (c) 18 month follow-up

contrast enhanced transverse CT image shows no enhancement in the involuted ablation zone (arrows).